Universal stretched exponential relaxation in nanoconfined water

Adarsh Shekhar, Rajiv K. Kalia, Aiichiro Nakano, Priya Vashishta, Camilla K. Alm, and Anders Malthe-Sørenssen

Articles you may be interested in

Nanoconfined water under electric field at constant chemical potential undergoes electrostriction
J. Chem. Phys. **140**, 074710 (2014); 10.1063/1.4865126

Anomalous composition-dependent dynamics of nanoconfined water in the interlayer of disordered calcium-silicates
J. Chem. Phys. **140**, 054515 (2014); 10.1063/1.4864118

On the molecular origin of high-pressure effects in nanoconfinement: The role of surface chemistry and roughness
J. Chem. Phys. **139**, 144701 (2013); 10.1063/1.4824125

Water dynamics in silica nanopores: The self-intermediate scattering functions
J. Chem. Phys. **136**, 224704 (2012); 10.1063/1.4724101

Structure and dynamics of water confined in silica nanopores
J. Chem. Phys. **135**, 174709 (2011); 10.1063/1.3657408

Universal stretched exponential relaxation in nanoconfined water

Adarsh Shekhar,[1] Rajiv K. Kalia,[1] Aiichiro Nakano,[1] Priya Vashishta,[1] Camilla K. Alm,[2] and Anders Malthe-Sørenssen[2]

[1]*Collaboratory for Advanced Computing and Simulations, Department of Physics & Astronomy, Department of Computer Science, and Department of Chemical Engineering & Materials Science, University of Southern California, Los Angeles, California 90089-0242, USA*
[2]*Department of Physics, University of Oslo, 0316 Oslo, Norway*

Understanding the behavior of water confined at the nanometer scale is a fundamental problem not only in physics but also in life sciences, geosciences, and atmospheric sciences. Here, we examine spatial and dynamic heterogeneities in water confined in nanoporous silica using molecular dynamics (MD) simulations. The simulations reveal intermixed low-density water and high-density water with distinct local structures in nanopores of silica. The MD simulations also show dynamic heterogeneities in nanoconfined water. The temporal decay of cage correlation functions for room temperature and supercooled, nanoconfined water is very well described by stretched exponential relaxation, $\exp(-(t/\tau)^\beta)$. The exponent β has a unique value, $d/(d+2)$, which agrees with an exact result for diffusion in systems with static, random traps in $d = 3$ dimensions. © 2014 AIP Publishing LLC. [http://dx.doi.org/10.1063/1.4899279]

The phase diagram of bulk water contains a supercooled region called the "no man's land (NML),"[1] see Fig. S1 in the supplementary material.[2] At ambient pressure, the NML lies between the homogeneous nucleation temperature $T_h \approx 235\,K$ and the glass transition temperature $T_g = 136\,K$. Below T_g, bulk water is frozen either as low-density amorphous (LDA) or high-density amorphous (HDA) ice. It has been suggested that these amorphous forms of ice become low-density water (LDW) and high-density water (HDW) in the NML.[3–5] Theoretical models have been proposed to account for anomalous enhancements in thermodynamics response functions, such as isothermal compressibility and specific heat at constant pressure, of supercooled water.[6] These models are based on (1) A liquid-liquid critical point scenario involving a transition between LDW and HDW phases terminating at a critical point;[7] (2) a singularity-free scenario arising from local density fluctuations;[8] and (3) a scenario hypothesizing a first-order transition sans the critical point between the two liquid phases.[9]

Experimental investigations of deeply supercooled water at ambient pressure are hampered by crystallization below the homogeneous nucleation temperature. In recent years, experimental[10–13] and computer simulation[14–16] studies have focused on the behavior of water confined in glasses, clays, glass capillaries, silica nanotubes, and thin films. Mallamace *et al.* studied supercooled water confined in a micelle-templated mesoporous silica (MCM-41-S) matrix.[17] Zhang *et al.* used neutron scattering to investigate liquid-liquid phase transition in deuterated water confined in nanopores of a MCM-41-S silica matrix.[18] Neutron scattering and NMR techniques have also been used to examine the dynamic behavior of supercooled, nanoconfined water.[19] These experiments indicate a breakdown of Stokes-Einstein relation in supercooled water confined in a nanotube or a lysozyme protein layer and also in a methanol mixture. This breakdown is attributed to dynamic heterogeneities,[20] which tend to decouple viscosity and diffusion below a certain temperature.

Here, we examine the structural and dynamical behavior of water in nanoporous silica. We performed all-atom molecular dynamics (MD) simulations with a reactive force field, which allows bond breaking and bond formation in silica and water. The force field consisted of pair-wise terms for charge transfer, steric repulsion, charge-dipole, and van der Waals interactions between atoms. Covalent interactions in the silica-water system were included through three-body terms. Details of the force field, including experimental validation, are given in the supplementary material.[2] MD simulations were performed in the microcanonical ensemble using periodic boundary conditions in x, y, and z directions. The equations of motion were integrated with the velocity-Verlet algorithm using a time step of 0.5 fs. The starting configuration of the system was chosen to be the β-cristobalite lattice because it has the same mass density as amorphous silica (a-SiO_2) under ambient conditions. The β-cristobalite lattice was heated to obtain a well-equilibrated liquid at temperature $T = 4500\,K$. Using uniform dilation, we obtained several molten systems at mass densities between 0.1 and 2.2 g/cc at $T = 4500\,K$. These expanded liquids were quenched and thermalized at room temperature to obtain nanoporous silica systems. The MD protocol for preparing nanoporous silica systems is discussed in the supplementary material (see also Fig. S2).[2]

Rapid changes in pressure due to expansion gave rise to cavitations in molten silica and the cavities were quenched as nanopores in the amorphous silica systems. Figure 1(a) is a snapshot of nanoporous silica at a mass density $\rho = 0.5$ g/cc. Here, the red regions represent silica and the pores are color coded to indicate their sizes. This nanoporous system has a wide range of pore shapes and sizes. We calculated the radii of gyration of nanopores to estimate their sizes and the moment-of-inertia tensor to characterize the shapes and anisotropies of nanopores, see the supplementary material.[2] Figure S3 shows distribution functions for pore shapes and pore anisotropies in the nanoporous silica system at $\rho = 0.5$ g/cc.[2]
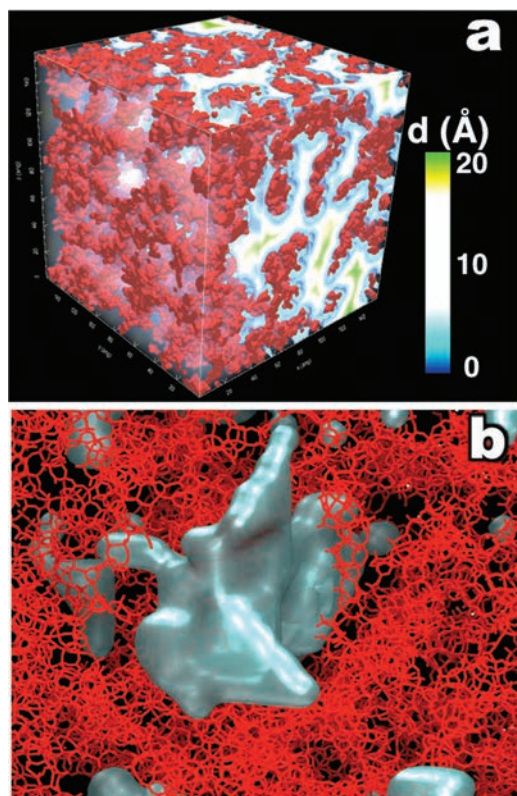
FIG. 1. Nanoporous silica synthesized *in-silico* by MD simulation. (a) The silica network, shown here in red, has an average mass density of 0.5 g/cc. In this network, each Si atom is four-fold coordinated with either O atoms or a combination of O atoms and -OH groups. The system has nanopores of various sizes, which are indicated here in blue, white, and green. (b) A snapshot showing a close-up view of the largest nanopore (gray and cyan) in the system. The radius of gyration, R_G, of the pore is 2.24 nm. The value of the shape parameter ($S = 0.33$) indicates that the nanopore is a prolate ellipsoid. The radius of gyration and shape parameter were calculated from the moment of inertia tensor, as described in the supplementary material.[2]

FIG. 2. Heterogeneous structure of water confined in nanoporous silica. Snapshot shows water molecules in nanopores of an amorphous silica system with an average mass density of 0.5 g/cc. The amorphous silica network is shown in red. Water molecules are color coded by mass density, which is calculated by Voronoi tessellation of oxygen atoms in water molecules. Dividing the mass of a water molecule by the volume of its Voronoi cell gives the mass density at the location of the molecule. The snapshot shows significant spatial heterogeneity in nanoconfined water. Blue and green dots indicate low-density water ($\rho < 0.9$ g/cc) and high-density water ($\rho > 1.1$ g/cc), respectively, and yellow represents water density between 0.9 and 1.1 g/cc.

Approximately 20% of the nanopores are spherical, 20% are oblate ellipsoids, and the rest are prolate ellipsoids. Figure 1(b) shows a close-up view of the largest nanopore (grey and cyan) and the surrounding Si-O network (red). The pore's radius of gyration is 2.24 nm and its anisotropy parameter $\Delta = 0.32$ and the value of the shape parameter ($S = 0.33$) indicates that this pore is a prolate ellipsoid.

Water molecules were embedded in nanopores of the amorphous silica (a-SiO$_2$) system after passivating the under-coordinated silicon atoms with –OH and dangling oxygen atoms with +H groups. The passivation protocol is discussed in the supplementary material.[2] Figure 2(a) is a snapshot of water molecules distributed in nanopores of the a-SiO$_2$ system at $\rho = 0.5$ g/cc and $T = 100$ K. Here, the silica network is again displayed in red. Blue and green dots represent water molecules with mass densities below 0.9 and above 1.1 g/cc, respectively, and yellow dots indicate water molecules with mass densities between 0.9 and 1.1 g/cc. Mass densities of water molecules in nanopores were obtained from the volumes of Voronoi cells[21] constructed around oxygen atoms of water molecules which were at least 1 nm away from the silica network. The mass-density distributions for water molecules exhibit thermal broadening but their overall shapes do not change significantly with temperature, see Fig. S4.[2]

We examined the nature of spatial heterogeneities in supercooled, nanoconfined water by analyzing the radial distribution functions, $g(r)$, for oxygen atoms in water molecules. Figure 3 shows $g(r)$ for LDW and HDW molecules at $T = 100$ K. Here, we chose a range of mass densities between 0.8 and 0.9 g/cc for LDW molecules and 1.1–1.3 g/cc for HDW molecules. This choice was guided by neutron scattering results[22] for mass densities of LDW and HDW (see below). We also calculated the tetrahedral order parameters and found that LDW and HDW molecules were four-fold coordinated. In Fig. 3, the first peaks in $g(r)$ for LDW and HDW are located at $r = 2.77$ and 2.85 Å, respectively. These peaks along with nearest-neighbor coordinations of four indicate the existences of first solvation shells in both LDW and HDW. The radial distribution function for LDW has a broad second peak around 4.2 Å, which indicates the presence of a second solvation shell. In contrast, the $g(r)$ for HDW has a peak around 3.4 Å and a shallow minimum around the second peak in the $g(r)$ for LDW. This behavior suggests that the second solvation shell of HDW molecules is broken. Additional evidence for an incomplete second solvation shell in HDW was found in the O-O-O bond-angle distribution calculated from the positions of oxygen atoms in HDW molecules. A complete second solvation shell would have given rise to a peak at 70°, whereas the MD calculation showed that the bond-angle distribution for HDW molecules was
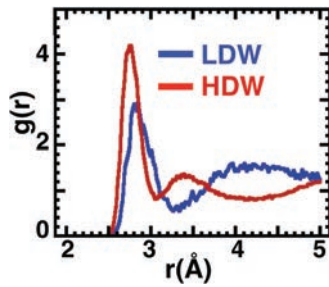
FIG. 3. Structural correlations in low-density and high-density water. Radial distribution functions, $g(r)$, for low-density water (blue curve labeled LDW) and high-density water (red curve labeled HDW) molecules in the nanoporous silica system at $T = 100$ K. Radial distribution functions were calculated from the positions of oxygen atoms of water molecules residing in nanopores of the silica network. Water molecules within 1 nm of the network atoms (silicon or oxygen in silica) were not included in the calculation. Here, the mass density of LDW ranges between 0.8 and 0.9 g/cc and the mass density of HDW lies between 1.1 and 1.3 g/cc. Areas under the first peaks indicate that both LDW and HDW molecules are four-fold coordinated and that their first solvation shells are complete. The second peak and second minimum in $g(r)$ for HDW are located near the first minimum and second peak in $g(r)$ for LDW molecules. These differences in local structures indicate that second solvation shells of LDW molecules are complete and those of HDW are disordered.

featureless. The second solvation shell in HDW is also absent at $T = 150$, 200, 250, and 300 K.

Our results for local molecular structures in LDW and HDW agree remarkably well with neutron scattering data of Soper and Ricci.[22] Using isotope substitution, they measured partial static structure factors of water as a function of pressure around the ice I/ice III triple point, which is at $T = 251$ K and pressure $P = 209$ MPa. With an increase in pressure from 26 to 400 MPa, they observed a continuous transformation from the LDW to HDW phase at $T = 268$ K. Assuming that the structure of water is a linear combination of the structures of LDW and HDW, they extracted from their data the mass densities of LDW and HDW to be 0.88 g/cc and 1.20 g/cc, respectively. Combining the measurements of oxygen-oxygen structure factors with simulations based on empirical pressure structure refinement, Soper and Ricci obtained radial distribution functions for LDW and HDW. They found the first peaks in $g(r)$ for LDW and HDW at 2.75 Å and the second peaks around 4.4 Å and 3.4 Å, respectively. Furthermore, the experimental radial distribution function for HDW showed a shallow minimum around 4.4 Å. These experimental results imply, in correspondence with our MD simulations, that the first and second solvation shells in LDW are complete and that the second solvation shell in HDW is not.

In addition to spatial heterogeneities, the MD simulations reveal dynamic heterogeneities in water confined in nanoporous silica. The mean square displacements of water molecules as a function of time show plateaus separating diffusive regimes, see Fig. S5 in the supplementary material.[2] These plateaus result from trapping of water molecules in cages formed by nearest-neighbor water molecules.[23] We examined the dynamics of water molecules through the cage correlation function

$$C(t) = \frac{\langle \sum_i l_i(t) \cdot l_i(0) \rangle}{\langle \sum_i l_i(0)^2 \rangle}, \quad (1)$$

where $l_i(0)$ and $l_i(t)$ are arrays containing information about the nearest neighbors of the ith water molecule at time $t = 0$ and at a later time t, respectively. The array elements are unity if the IDs correspond to nearest neighbors of the ith molecule at that time; otherwise, they are set equal to 0. On average, this function gives the fraction of nearest neighbors retained by the ith water molecule after time t. The cage correlation functions were calculated for water molecules, which were at least 1 nm away from the surfaces of silica nanopores, see Fig. S6 in the supplementary material.[2] Figures 4(a) and 4(b) show how $C(t)$ decays at $T = 200$ and 250 K. These curves, along with the MD results for cage correlation functions at other temperatures, collapse into a single curve when the data are plotted against t/τ; see Fig. 4(c). The Kohlrausch-Williams-Watts[24,25] or stretched exponential relaxation $\exp(-(t/\tau)^{\beta})$ with $\beta = 0.6$ provides the best fit to cage correlation functions for nanoconfined water at all temperatures. The relaxation time, τ, increases significantly upon cooling. The value of β coincides with an exact asymptotic relation for diffusion in a system with static random traps, namely, $\beta = d/(d+2)$, where $d = 3$ is the spatial dimensionality of the system.[26,27] We interpret this as an effect of the nanoporous silica network, which effectively provides a set of static traps for water molecules diffusing in its nanopores.
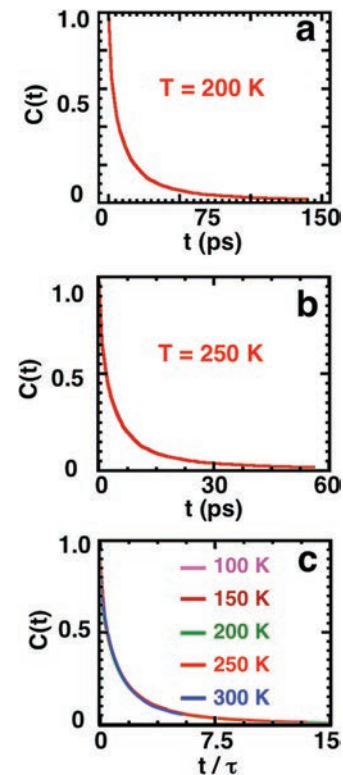
FIG. 4. Stretched exponential relaxation of nanoconfined water. Temporal decay of cage correlation functions, $C(t)$, for water molecules in nanoporous silica. The decay in $C(t)$ provides a measure of the average residence time of water molecules trapped in cages formed by nearest neighbor water molecules. Panels (a) and (b) show that $C(t)$ decays more slowly and the cage residence time increases upon cooling. These curves were fitted to stretched-exponential relaxation, $\exp(-(t/\tau)\beta)$. Panel (c) shows that the MD results for $C(t)$ versus t/τ at $T = 100$, 150, 200, 250, and 300 K collapse into a single curve. The value of the shaping exponent, $\beta = 0.6$, agrees with an exact theoretical result, $\beta = d/(d+2)$, for diffusion in a medium with static, random traps in $d = 3$ spatial dimensions.

In conclusion, the MD simulations reveal that the nanoporous silica network induces spatial heterogeneities in the form of LDW and HDW. The MD simulations indicate that the first and second solvation shells of LDW are fully formed, whereas the second solvation shell of HDW molecules is disordered. These local structural differences in LDW and HDW are akin to those observed in neutron scattering experiments.[22] The simulations also indicate that the nanoporous silica network instigates dynamic heterogeneities, which are manifested as a "universal" stretched exponential relaxation of cage correlation functions for water molecules. The shaping exponent in the stretched exponential function has a unique value, $\beta = 3/5$, which Phillips calls a "magic" number.[28] Experiments support the existence of dynamic heterogeneities in supercooled liquids[29] and theoretical work indicates that they arise from inherent structures in the energy landscape of undercooled liquids.[30] NMR[31] and neutron scattering experiments may be able to probe the dynamics of water confined in nanoporous silica, see also Fig. S7.[2] These features of nanoconfined water are quite general and therefore relevant to other systems including, but not limited to, nanostructures in cement,[32] conformational dynamics of proteins,[33] and material transport in nanogeoscience.[34]

[1] O. Mishima and H. E. Stanley, Nature **396**(6709), 329–335 (1998).
[2] See supplementary material http://dx.doi.org/10.1063/1.4899279 for simulation details.
[3] H. E. Stanley, S. V. Buldyrev, O. Mishima, M. R. Sadr-Lahijany, A. Scala, and F. W. Starr, J. Phys. Condens. Matter **12**(8A), A403–A412 (2000).
[4] C. Huang, K. T. Wikfeldt, T. Tokushima, D. Nordlund, Y. Harada, U. Bergmann, M. Niebuhr, T. M. Weiss, Y. Horikawa, M. Leetmaa, M. P. Ljungberg, O. Takahashi, A. Lenz, L. Ojamae, A. P. Lyubartsev, S. Shin, L. G. M. Pettersson, and A. Nilsson, Proc. Natl. Acad. Sci. U.S.A. **106**(36), 15214–15218 (2009).
[5] A. Nilsson, C. C. Huang, and L. G. M. Pettersson, J. Mol. Liq. **176**, 2–16 (2012).
[6] R. J. Speedy and C. A. Angell, J. Chem. Phys. **65**(3), 851–858 (1976).
[7] P. H. Poole, F. Sciortino, U. Essmann, and H. E. Stanley, Nature **360**(6402), 324–328 (1992).
[8] S. Sastry, P. G. Debenedetti, F. Sciortino, and H. E. Stanley, Phys. Rev. E **53**(6), 6144–6154 (1996).
[9] C. A. Angell, Science **319**(5863), 582–587 (2008).
[10] M. C. Bellissentfunel, J. Lal, and L. Bosio, J. Chem. Phys. **98**(5), 4246–4252 (1993).
[11] R. Bergman and J. Swenson, Nature **403**(6767), 283–286 (2000).
[12] P. Smirnov, T. Yamaguchi, S. Kittaka, S. Takahara, and Y. Kuroda, J. Phys. Chem. B **104**(23), 5498–5504 (2000).
[13] U. Raviv, P. Laurat, and J. Klein, Nature **413**(6851), 51–54 (2001).
[14] P. Gallo, M. Rovere, and S. H. Chen, J. Phys. Chem. Lett. **1**(4), 729–733 (2010).
[15] D. T. Limmer and D. Chandler, J. Chem. Phys. **137**(4), 044509 (2012).
[16] N. H. de Leeuw, Z. M. Du, J. Li, S. Yip, and T. Zhu, Nano Lett. **3**(10), 1347–1352 (2003).
[17] F. Mallamace, M. Broccio, C. Corsaro, A. Faraone, D. Majolino, V. Venuti, L. Liu, C. Y. Mou, and S. H. Chen, Proc. Natl. Acad. Sci. U.S.A. **104**(2), 424–428 (2007).
[18] Y. Zhang, A. Faraone, W. A. Kamitakahara, K. H. Liu, C. Y. Mou, J. B. Leao, S. Chang, and S. H. Chen, Proc. Natl. Acad. Sci. U.S.A. **108**(30), 12206–12211 (2011).
[19] F. Mallamace, C. Branca, C. Corsaro, N. Leone, J. Spooren, H. E. Stanley, and S. H. Chen, J. Phys. Chem. B **114**(5), 1870–1878 (2010).
[20] L. M. Xu, F. Mallamace, Z. Y. Yan, F. W. Starr, S. V. Buldyrev, and H. E. Stanley, Nat. Phys. **5**(8), 565–569 (2009).
[21] C. H. Rycroft, Chaos **19**(4), 041111 (2009).
[22] A. K. Soper and M. A. Ricci, Phys. Rev. Lett. **84**(13), 2881–2884 (2000).
[23] E. Rabani, J. D. Gezelter, and B. J. Berne, Phys. Rev. Lett. **82**(18), 3649–3652 (1999).
[24] G. Williams and D. C. Watts, Trans. Faraday Soc. **66**(565P), 80 (1970).
[25] M. D. Ediger, C. A. Angell, and S. R. Nagel, J. Phys. Chem. **100**(31), 13200–13212 (1996).
[26] M. Donsker and S. Varadhan, Commun. Pure Appl. Math. **32**, 721–747 (1979).
[27] P. Grassberger and I. Procaccia, J. Chem. Phys. **77**(12), 6281–6284 (1982).
[28] J. C. Phillips, Rep. Prog. Phys. **59**(9), 1133–1207 (1996).
[29] M. T. Cicerone and M. D. Ediger, J. Chem. Phys. **103**(13), 5684–5692 (1995).
[30] P. G. Debenedetti, T. M. Truskett, C. P. Lewis, and F. H. Stillinger, Adv. Chem. Eng. **28**, 21–79 (2001).
[31] R. Bohmer, G. Diezemann, G. Hinze, and E. Rossler, Prog. Nucl. Mag. Res. Spectrosc. **39**(3), 191–267 (2001).
[32] H. M. Jennings, Cement Concrete Res. **38**(3), 275–289 (2008).
[33] S. Bockenhauer, A. Furstenberg, X. J. Yao, B. K. Kobilka, and W. E. Moerner, J. Phys. Chem. B **115**(45), 13328–13338 (2011).
[34] M. F. Hochella, Elements **4**(6), 373–379 (2008).